THE JOURNAL OF PHYSICAL CHEMISTRY B

B: Liquids, Chemical and Dynamical Processes in Solution, Spectroscopy in Solution

Experimental and DFT Studies of Hybrid Silver/Cdots Nanoparticles

Jeison Manuel Arroyave, Ruben Eduardo Ambrusi, María Estela Pronsato, Alfredo Juan, Marcelo Fabián Pistonesi, and María Eugenia Centurión

J. Phys. Chem. B, **Just Accepted Manuscript** • DOI: 10.1021/acs.jpcb.9b10430 • Publication Date (Web): 05 Mar 2020

1

Experimental and DFT Studies of Hybrid Silver/Cdots Nanoparticles

Jeison Manuel Arroyave,[1] Rubén E. Ambrusi,[2] María Estela Pronsato,[2] Alfredo Juan[2], Marcelo Fabian Pistonesi,[1] María Eugenia Centurión[1]

[1] INQUISUR, Department of Chemistry, Universidad Nacional del Sur, Av. Alem 1253, B8000CPB, Bahía Blanca, Argentina

[2] IFISUR, Department of Physics, Universidad Nacional del Sur, Av. Alem 1253, B8000CPB, Bahía Blanca, Argentina

*Corresponding author: mecentur@criba.edu.ar

ABSTRACT

In this work, the combination of experimental and theoretical results was employed to confirm an interaction between Cdots and AgNPs in the silver/Cdots hybrid nanoparticles. The experimental data obtained by UV Vis, IR, zeta potential and TGA techniques were correlated and interpreted by calculations obtained by DFT. Particularly, an interaction between the -COO^- functional group of the Cdots with AgNPs was revealed. As consequence of this interaction, a frequency shift and a higher absorption intensity in the IR of the –OH group in the Cdots was theoretically predicted and also observed in the experimental IR spectra. Moreover a bonding and charge distribution analysis was also carried out. These results constitute new physical insight for Ag@Cdots system. Additionally, based in this type of interaction, energy calculations explained the negative charge surrounding the AgNPs, which was detected by zeta potential measurements. This systematic methodology is not only useful for this nanoparticles system, but could also be used to analyze the interaction between the components that constitute other types of hybrid nanoparticles.

1. INTRODUCTION

The nature of nanomaterials is significantly different from that of bulk solids as regards their optical, thermal, electrical, magnetic, mechanical and chemical aspects [1]. Nanomaterials have special structural properties due to the effect of their small size, surface effect, quantum size effect, etc. Carbon is usually a black material, commonly considered to have little fluorescence and low water solubility. Due to its good optical properties, like luminescence and good water solubility, carbon-based quantum dots (Cdots) have received extensive attention [2,3]. Not only are they easier to synthesize on a large scale and with low cost but they also stand out due to many of their properties, such as their excellent conductivity, high chemical stability, respect for the environment, wideband optical absorption, low toxicity, strong photoluminescence emission and optical properties. The surface of the Cdots exhibits chemical functional groups connected or modified, such as groups based on oxygen and amino. Most carboxyl group residues on the surface of Cdots provide great water solubility and biocompatibility [4]. These surface and structural characteristics determine their various characteristics, and this depends on the various methods of synthesis. For example, in the bottom up methods, the Cdots are synthesized from polycyclic aromatic compounds through the processes of dehydration and carbonization. There are several techniques used for the processes of dehydration and carbonization; among them, the hydrothermal [5], carbonization in a micro-reactor [6], microwave-hydrothermal [7] and plasma-hydrothermal [8] methods. These methods allow excellent control of the properties of the final product.

On the other hand, silver nanoparticles (AgNPs) have also attracted great interest thanks to their optical properties [9,10]. At present, due to their unique physical and chemical properties (optical, electrical and thermal, high electrical and biological conductivity), they are being increasingly used in various fields which include medical, food, health, consumer and industrial purposes [11–13]. The nature of the AgNPs surface depends on the synthesis method used. Gonzalez *et. al.* [14] reported on the synthesis of AgNPs from glucose and was able to explain the role of D-glucose and D-gluconate ions on their surface (Capping) using Raman and density functional theory (DFT) studies.

To improve the properties of different nanomaterials or to provide a synergistic effect, hybrid nanoparticles consisting of two or more types of individual nano components are emerging. For example, it has been shown that the Cdots are suitable for surface passivation and chemical modification with various polymeric, organic or inorganic materials, such as AgNPs. The physical and fluorescence characteristics can be improved by the passivation of the surface to determine glucose in human serum [15]. Lu *et al*. developed a novel Ag@CQDs core/shell nanoparticles for electrochemiluminescence detection of Cl− ion in in tap water and human serum samples [16]. A fluorescence sensor for sensitive and selective detection of iodide using carbon nanodots/silver nanocomposites was developed [17]. Moreover, metal@Fe_2O_3 composites were obtained to evaluated the catalytic performances by monitoring the reduction of p-nitrophenol and photodegradation of methylene blue [18]. Therefore, an adequate characterization is required, not only to validate the efficiency of the procedures by which they are obtained but also to know the type of interactions that occur between this kind of nanoparticles. A precise characterization of the particles is necessary since the physicochemical properties of a particle could have a significant impact on its properties. To evaluate these aspects, many analytical techniques have been used, including visible ultraviolet spectroscopy (UV-vis spectroscopy), X-ray diffractometry (XRD), Fourier transform infrared spectroscopy (FTIR), X-ray photoelectron spectroscopy (XPS), dynamic light scattering (DLS), scanning electron microscopy (SEM), transmission electron microscopy (TEM), atomic force microscopy (AFM), etc [7,16,17].

Ab initio methods were applied extensively in the study of infrared (IR) spectroscopy properties on different systems [18–20]. Edge functionalized graphene quantum dots was studied by quantum-chemical calculations, determining vibrational spectra for different functional groups, but using a coronene model to represent Cdots [21]. Dispersion interaction and IR absorption spectroscopy was studied both experimentally and theoretically for adsorbed water molecules on the epoxide groups of graphene oxide surfaces [22]. Nevertheless, to our knowledge IR vibrational spectra of Ag@Cdots has not been studied theoretically yet. Recently we performed a theoretical approach in order to model these type structures with polycyclic aromatic molecules and Ag cluster [23], focusing mainly

on the stability of these structures and UV-visible spectra. In that work, the investigation of Gonzales *et al.* [14] was continued to comprehend the interaction of AgNPs synthesized by D-glucose with Cdots structures. In this sense, the use of polycyclic aromatic molecules was used to build the Cdot using the Hückel rule for the hydrocarbon core with the addition of different functional groups to calculate UV-visible spectrum which match well with experimental spectra reported in literature. Such a process is useful to develop a reliable model to represent Cdots structures. However, a study of the IR spectra and the influence of silver on Cdots vibration frequencies and absorption intensity are still not investigated. The evaluation of these properties is not a minor issue in a system where the species are present in very low concentration (diluted systems). In this case the thermodynamic energy calculations are not enough to determine if an effective interaction between the species involved occurs. The present theoretical and experimental methodology becomes relevant to achieve concluding evidence in favor or against the interaction between Cdots and AgNPs during the formation of hybrid Cdot@Ag structures. Moreover, a study of the bonding involved in this process was also carried out.

It is necessary and important to implement new tools for the characterization of nanoparticles obtained by new synthesis methods. In this work, hybrid nanoparticles of Carbon and Silver (Ag@Cdots) will be characterized for which it will be necessary to characterize the nanoparticles individually. The AgNPs will be synthesized using glucose as a reducing and stabilizing agent. The Cdots and Ag@Cdots will be synthesized through "bottom up" methodologies, using glucose as a precursor and under microwave heating.

Combined traditional characterization techniques (UV-Vis, IR, zeta potential and TGA) will be used with theoretical calculations for the analysis of the interaction of Ag@Cdots surfaces. This type of studies were not found in the literature. The correlation of the information obtained will enable to characterize in more detail the interaction between AgNPs and Cdots in Ag@Cdots. It is worth highlighting the value and potential of using combined experimental and theoretical data as a useful tool to understand the interaction not only of Ag@Cdots but also of other nanostructured hybrid materials.

2. METHODOLOGY

2.1. Reagents

All reagents were of analytical grade and solutions were prepared using ultrapure water (18 MΩ). A silver solution of $AgNO_3$ (Merck 99.9%). Sodium hydroxide (Anedra, Argentina). Glucose was obtained from Sigma-Aldrich (Germany).

2.2. Synthesis Silver Nanoparticles (AgNPs)

AgNPs were synthesized as described by González Fá *et al.* [24]. In a typical procedure, 5.88 mM $AgNO_3$ (2.65 µL) were mixed with 7.82 g L^{-1} glucose (40 µL/0.31 g L^{-1}). The pH was adjusted to 10.0 with sodium hydroxide solutions (0.1 M) and taken to 10.0 mL with water with intense agitation for 60 seconds. The AgNPs average size was 10 nm

2.3. Synthesis of Carbon dots (Cdots) and Carbon/Silver hybrid nanoparticles (Ag@Cdots)

Cdots and Ag@Cdots were synthesized as described by Arroyave *et al.* [7]. First of all, for Cdots synthesis, 0.31 g L^{-1} glucose (3 mL) at pH 10 (by addition of NaOH 0.1 M) was transferred to a 10 mL tube. The reactants reacted at 350 W during 60 seconds under a conventional microwave treatment. A typical Cdots brown color was observed. To synthesize Ag@Cdots 3 mL of a solution that contains glucose and $AgNO_3$ (0.31 g L^{-1} of glucose and $AgNO_3$ of 1.56x 10^{-4} M) at pH 10 were exposed to a conventional microwave treatment at 350 W during 60 seconds. The Cdots and Ag@Cdots average sizes obtained were 8 and 12 nm respectively.

2.4. Synthesis of nanoparticles varying glucose concentration

Since glucose is the source of Cdots synthesis, the effect of the variation in glucose concentration in a range between 0.15 and 0.63 g L^{-1} was studied.

2.5. Characterization of Nanoparticles

The nanoparticles were characterized by the surface plasmon resonance bands (SPRB), Molecular Fluorescence (PL), Transmission electron microscopy (TEM), Hydrodynamic size and zeta potential, Thermogravimetric analysis (TGA), X-ray diffraction (XRD) and ATR-FTIR spectroscopy.

2.5.1. Comparison between the characterization and theoretical calculations

We will focus on the analysis of the results obtained by the surface plasmon resonance bands (SPRB), ATR-FTIR spectroscopy, Thermogravimetric analysis (TGA) and Zeta Potential.

2.6. Theoretical calculations

DFT calculations were performed using the Vienna Ab initio Simulation Package (VASP) [25,26], which employs a plane-wave basis set and a periodic supercell method. The generalized gradient corrected approximation (GGA) functional of Perdew, Burke, and Ernzerhof (PBE) was used [27]. The Kohn–Sham equations were solved variationally using the projector-augmented-wave (PAW) method [28,29]. The expansion of the plane-wave basis set was performed with a cutoff energy of 400 eV. The sampling of the reciprocal space was performed using the gamma-centered Monkhorst–Pack scheme [30] with 1x1x1 kpoints grid for the integration over the Brillouin zone. Partial occupations for the electronic states near the Fermi level were obtained by Gaussian smearing approach, with a 0.2 eV smearing width.

Total energy was minimized performing a geometry relaxation in the supercell to obtain the optimized structures using a conjugated gradient algorithm to relax ions [31], until it converged within 10^{-4} eV and the forces on each ion were less than 0.01 eV $Å^{-1}$. van der Waals interactions were taken into account by the

Grimme's DFT-D2 method, which is optimized for several DFT functionals [32]. After performing the geometry optimization with PBE functional including dispersion interactions on all structures, a hybrid functional was considered for the electronic structure at B3LYP level [33] and the solvent effect was included by applying VASPsol package [34,35] for energies, vibrational calculations and partial density of states (PDOS).

All Cdots calculations were performed in a 30x30x30 Å box, following the model proposed in a previous work [23]. Variations of this model were introduced, but keeping the use of a three silver atom triangular cluster to evaluate the properties of silver nanoparticles and its interactions with Cdots. This cluster size has demonstrated to be a good approximation for calculating the adsorption energies of glucose and gluconate ions on silver nanoparticles [14,23]. This assumption confirmed in previous works, is based on Recka *et al.* work [36], which shows that major size clusters can be build up by Ag_3 basic units. Growing larger structures by aggregation of these small units is more stable than by addition of single atoms.

Adsorption energy (E_{ads}) calculations were performed by the use of Eqn (1), which was applied for both, molecule or Cdot, on the silver nanoparticle

$$\mathrm{E_{ads}} = \mathrm{E(Ag_3 + molecule\ (or\ Cot))} - \mathrm{E(Ag_3)} - \mathrm{E(molecule\ (or\ Cdot))} \quad (1)$$

where E(Ag_3+molecule (or Cdot)), E(molecule (or Cdot)) and E(Ag_3) are the total energies of the molecule (D-glucose or D-gluconate) or Cdot adsorbed on Ag_3 cluster, the isolated Ag_3 cluster, and the isolated molecule or Cdot respectively. With this definition negative adsorption energies correspond to a stable adsorption of the molecules or Cdot on the silver surface. The interaction between species and the mechanism involved in the stability of the main structures was carried out analyzing the bonding between atoms. The overlap population (OP) concept in extended structures (OPDOS) [37,38], and Bond Order (BO) as implemented in the DDEC6 method [39–41] were employed. In addition an orbital analysis of the highest occupied molecular orbital (HOMO) and lowest

unoccupied molecular orbital (LUMO), and density difference isosurfaces was also performed.

Frequency calculation was performed at the harmonic limit, for normal modes from the DFT surface potential energy [42]. In addition the IR absorption intensity of the *i*th vibrational mode is given by the use of equation of equation (2) [43,44].

$$I_i^{IR} = \frac{N\pi}{3c}\left|\frac{d\boldsymbol{\mu}}{dQ_i}\right|^2 \quad (2)$$

In this equation, *N* is the number of Cdots or molecules per unit volume, $\boldsymbol{\mu}$ is the cluster dipole moment, and Q_i is the normal coordinate corresponding to the ith mode [45].

By applying equation (2), we evaluate the relative intensity for the *i*th vibrational mode,

$$I_i^{rel} = \frac{I_i^{IR-adsorbed}}{I_i^{IR-isolated}} \quad (3)$$

where $I_i^{IR-adsorbed}$, is the intensity for the *i*th vibrational mode of the adsorbed Cdots or molecules on Ag_3 cluster, and $I_i^{IR-isolated}$ is the intensity for the same vibrational mode obtained for isolated Cdots, for the same value of *N*.

3. RESULTS AND DISCUSSION

3.1. Characterization of Nanoparticles

3.1.1. UV-Vis spectroscopy

The optical properties of the synthesized nanoparticles (AgNPs, Cdots, and Ag@Cdots) were characterized by UV-Vis spectroscopy. AgNPs show a characteristic SPRD in the visible region of the spectrum (black line) for this type of nanomaterials and absorption band at 410 nm [24]. Cdots present an absorption band at 265 nm and one shoulder at 338 nm [7], probably due to the presence of

carboxylate groups (COO^-) in the surface [23]. On the other hand, Ag@Cdots presents an absorption band at 265 nm due Cdots contribution and an absorption band at 410 nm due to AgNPs.

3.1.2. Thermogravimetric analysis (TGA)

Thermogravimetric analysis of Cdots and Ag@Cdots was studied by Arroyave *et al.* [7]. At the first stage, up to 180 ºC, similar behavior can be observed for the three nanoparticle materials. A decrease in the initial mass of approximately 29% due to the evaporation of superficial water, both free and bound, was observed. In a second stage, between 180 ºC and 390 ºC the Cdots and Ag@Cdots have a total weight loss of about 62%. The weight loss is probably due to the decomposition of labile oxygen functional groups located at the surface of the Cdots [7]. In the third and last stage, there is a difference in the rate of weight loss between 390 y 1000 ºC; this suggests that there could be an interaction between the Cdots and AgNPs. This is in agreement with the higher stability found for Cdots in the presence of silver, based on the adsorption energies calculated in this work, and the stability analysis performed in our previous work [23].

3.2. Characterization of Nanoparticles: Study of the effect of glucose concentration on nanoparticles

3.2.1. UV-Vis spectroscopy

Figure 1 shows AgNPs, Cdots and Ag@Cdots SPRD synthesized with different glucose concentrations. **Figure 1 (a)** shows that as the concentration of glucose increases from 0.15 (black line) to 0.63 g of glucose L^{-1} (red line), the band at 410 nm becomes narrower. This indicates a lower aggregation between the nanoparticles due to the coating formed by glucose [24,46]. A 280 nm band is observed due to prismatic AgNPs [14].

Cdots SPRDs shown (**Figure 1 (b)**), a proportional increase in intensity at 265 and 338 nm with an increase of glucose concentration [7]. Speaking specifically of the band at 338 nm, as stated above, this can be attributed to groups (COO^-). It is also observed that at the lowest glucose concentration the Cdots are not formed.

The same applies to Ag@Cdots (**Figure 1 (c)**). The concentration of glucose during synthesis increases the intensity of the bands at 265, 338 and 410 nm, which means that a higher concentration of the synthesized nanoparticles were obtained. It is consistent with the fact that with high glucose concentration, more Cdots will be obtained. In addition, these Cdots bind to the surface of the AgNP and stabilize them. AgNPs have glucose and D-Gluconate molecules on their surface [14], which can be displaced and/or converted into Cdots after microwave heating [7,23].

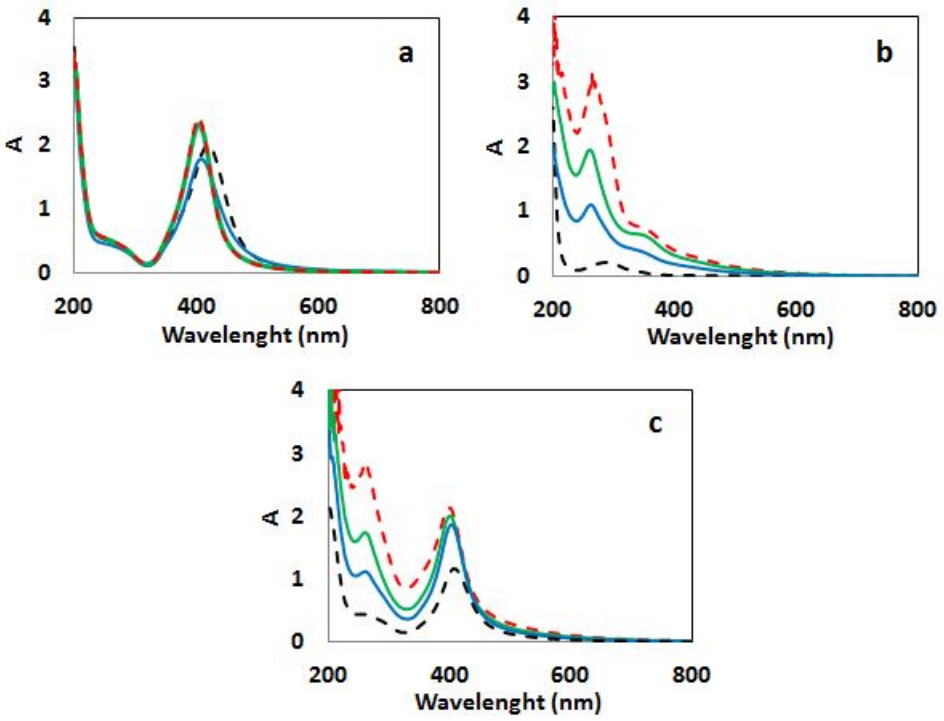

Figure 1. SPRD of nanoparticles synthesized with different glucose concentrations: **(a)** AgNPs, **(b)** Cdots and **(c)** Ag@Cdots. 0.15 g L^{-1} (black), 0.31 g L^{-1} (blue), 0.49 g L^{-1} (green) and 0.63 g L^{-1} (red)

3.2.2. ATR-FTIR spectroscopy

AgNPs, Cdots and Ag@Cdots FTIR spectra synthesized with different glucose concentrations are shown in **Figure 2**. The region between 950 and 1800 cm^{-1} will be analyzed, due to the chemical bonds of interest are found. In all cases, using different concentrations of glucose in the synthesis (**Figure 2 (a)** - **Figure 2 (d)**), characteristic peaks of the vibrations C = O (aromatic) and C = C are observed, between 1710 cm^{-1} and 1500 cm^{-1}. The peaks between 1000 and 1400 cm^{-1} correspond to the stretching of C-OH and the vibration of flexion of OH, due to the residual hydroxy groups on the surface of Cdots and Ag@Cdots. These groups are generated due to dehydration, decarboxylation and aromatization of glucose [47].

The spectra of Cdots and Ag@Cdots show differences in the intensities of 1730 cm^{-1} and 1000 cm^{-1} that correspond to the group C=O and C-O, respectively [47,48]. These bands tend to decrease the transmittance by increasing the concentration of glucose used in the synthesis of the nanoparticles, particularly in the region between 1000 and 1010 cm^{-1}. It can be seen that the Cdots have higher transmittance compared to AgNPs and Ag@Cdots. On the other hand, a decrease in the intensity in the band around 1250 cm^{-1} (corresponding to the C-O and C-OH groups) was also detected, for AgNPs and Ag@Cdots, while for the Cdots this band does not observed [49]. For this reason, such spectral changes suggest an interaction between the surfaces of the nanoparticles and Cdots; otherwise, the spectra of Cdots and Ag@Cdots would have to be similar.

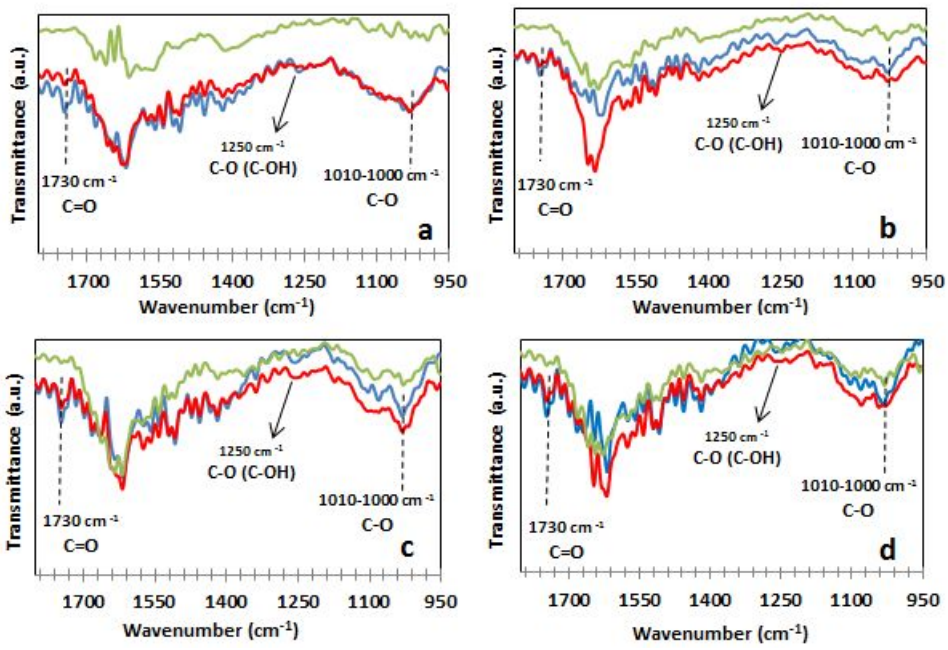

Figure 2 FTIR spectra of AgNPs (blue), Cdots (green) and Ag@Cdots (red) synthesized with different glucose concentrations: **(a)** 0.15 g L^{-1}, **(b)** 0.31 g L^{-1}, **(c)** 0.49 g L^{-1} and **(d)** 0.63 g L^{-1}

3.2.3. Zeta Potential

AgNPs, Cdots and Ag@Cdots zeta potential values synthesized with different glucose concentrations are shown in **Figure 3.** AgNPs zeta potential values are more negative with high glucose concentration (from -27.3 to -43 mV). This occurs due to the generation of gluconate from glucose on the surface, which gives it negative charges [14]. As for the Cdots, there is no significant change in their zeta potential with the variation in glucose concentration; they have an average value of -14 mV. In this case, the negative values are due to the destruction of some of the glucose functional groups in the synthesis of Cdots [50]. For Ag@Cdots, a decrease in zeta potential (from -30.7 to -16.9 mV) is observed as the concentration of glucose used in the synthesis increases. This trend suggests that the formed Cdots could be interacting with AgNPs. When 0.63 g L^{-1} of glucose is used, a greater amount of Cdots is expected to be obtained and therefore a greater surface interaction with AgNPs, which changes the negative charges of the nanoparticle, obtaining intermediate values of zeta potential with

respect to AgNPs and Cdots values obtained [50–52]. In this case, Ag@Cdots zeta potential (-16.9 mV) is closer to Cdots zeta potential values (-14 mV). The zeta potential results obtained provide valuable complementary information on the surface interaction of these nanoparticles.

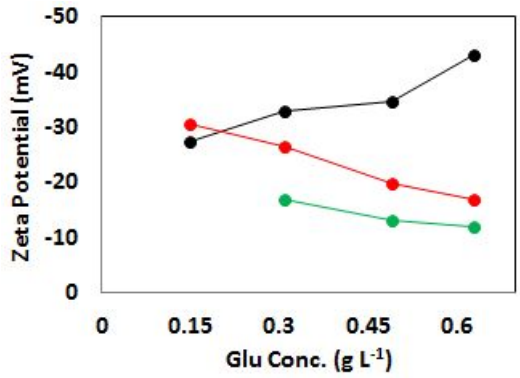

Figure 3 Potential Zeta values of nanoparticles synthesized with different glucose concentrations. AgNPs (black), Cdots (green) and Ag@Cdots (red)

When the concentration of glucose increases apparently Cdots are formed on silver yielding to Ag@Cdots but also isolated ones. For that reason the Zeta potential become less negative. At a glucose concentration of 0.15 gL^{-1}, isolated Cdots are not formed as can be observed in the green curve, in agreement with the UV-visible spectra, and the Ag@Cdots zeta potential is more negative than the AgNPs. This behavior is consistent with that suggested by Ambrusi *et. al.* [23]. According to these calculations, a Cdot can replace a glucose molecule adsorbed on AgNPs when it interacts with $–COO^-$ group, but cannot replace the gluconate ion. Therefore, this process generates an increment in the amount of negative charge for Ag@Cdots compared with AgNPs. As the concentration of glucose increases, not only Ag@Cdots are formed but also isolated Cdots, consequently the average negative charge surrounding these structures tends to the isolated Cdots zeta potential value.

3.3. Theoretical calculations

Based on a previous work [23], we propose different structures to evaluate how the interactions with silver can affect the normal vibrational modes of different functional groups, belonging to Cdots. A similar analysis was also performed for α-glucose and D-gluconate ion, which are molecules that act as

capping agents in silver nanoparticles [14]. The oxygenated functional groups considered, are evaluated in the case of direct interaction with silver, and also when they are not bound directly to the silver. For the latter case, they belong to a Cdot (or molecule) that interacts through another equal or different functional group with silver. This slight modification of the model compared to our previous work [26], obeys to an attempt to evaluate the effect that the interaction of one functional group can have on the frequency and/or intensity of absorption of another group, which is a probable stage since it is not expected that all functional groups will interact with the silver surface.

Because it is extremely difficult to contemplate all possible stages and also to determine experimentally which case is more probable, in this attempt we have started by considering the most simple ones, developing a heuristic that was finally accepted based also on the capability to interpret experimental results. Despite its simplicity, the calculation for a single functional group still constitutes a useful case, because it represents the special case of a minimal adsorption energy, which can increase if more functional groups are adsorbed. On the other hand, the energy is not the only relevant property of the system. Some features of the IR spectra were also predicted for the case of isolated or hybrid structures.

Figure 4 shows the optimized structures included in the calculation. The nomenclature used for Cdots indicates the functional group added to represent its surface. For the adsorbed structures (Cdots or molecules) on Ag_3 cluster, the functional group in parenthesis represents the one which interacts with silver. In the case of Cdots, additionally the functional group unbound with silver is denoted without parenthesis.

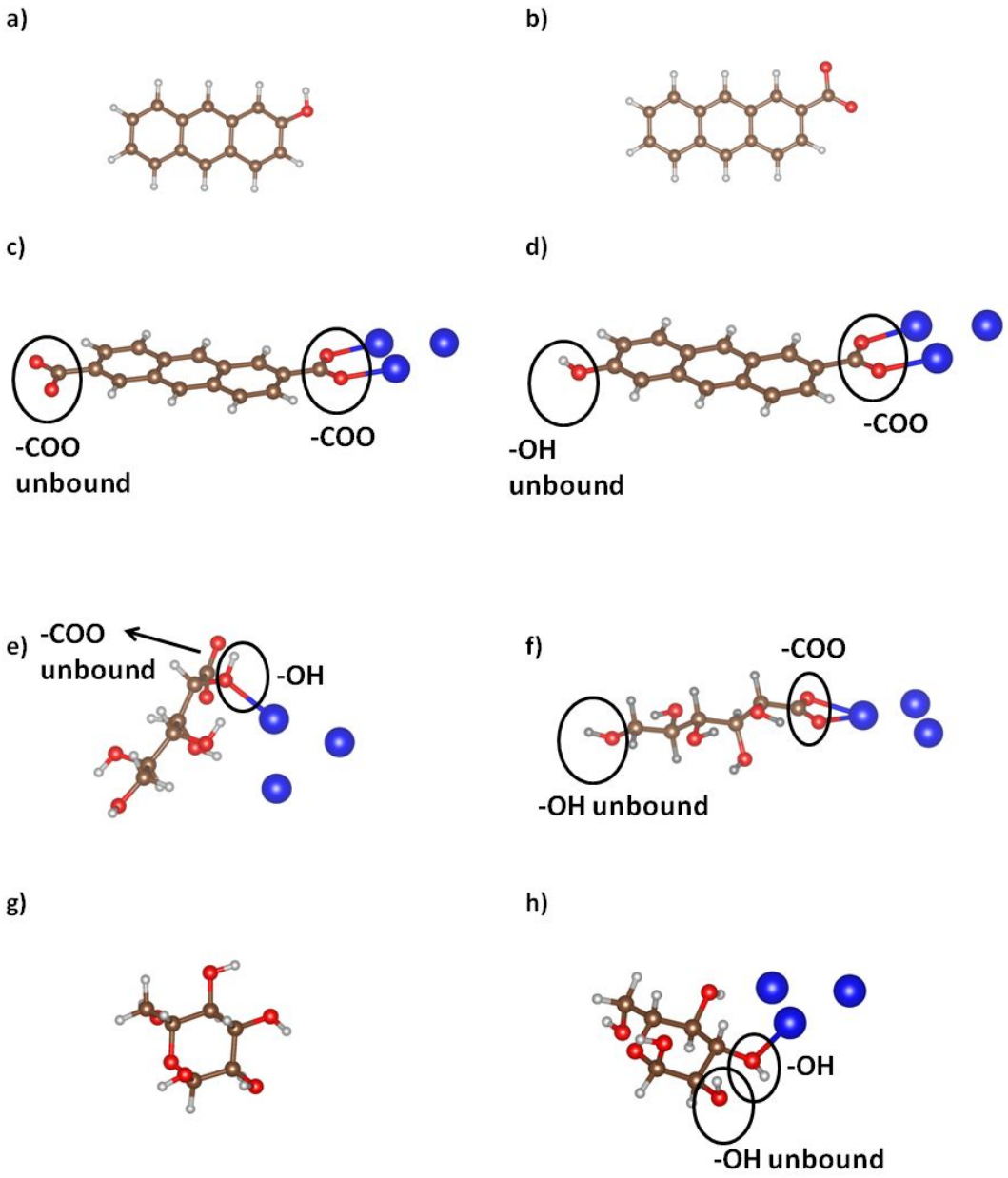

Figure 4 Employed structures for DFT calculations of Cdot and Ag@Cdot structures, and molecules involved in the synthesis; a) Cdot-OH, b) Cdot-COO, c) COO-Cdot(-COO)-Ag_3, d) OH-Cdot(-COO)-Ag_3, e) D-gluconate(-OH)-Ag_3, f) D-gluconate(-COO)-Ag_3, g) α-D-glucose and h) α-D-glucose-Ag_3

As mentioned earlier, the stability of the different systems were evaluated calculating adsorption energies. To interpret these adsorption energies it is crucial to focus on the experimental fact that D-gluconate and D-glucose molecules are both adsorbed on AgNPs surface acting as capping agents during

the synthesis of AgNPs through D-glucose. Consequently, it is relevant and innovative to determine if there is an interaction between silver and Cdots during the formation of Ag@Cdots structures or if the Cdot is formed isolated in the solution without interacting with AgNPs. For that reason, the calculations attempt to evaluate the adsorption strength necessary for a stable replacement of D-glucose or D-gluconate by Cdots, which is fundamental to have an interaction between Cdots and AgNPs.

Cdots structures appear to be more stable in the presence of silver [23], especially when Cdots interact with silver through the –COO oxygenated functional group. Calculated adsorption energies of OH-Cdot(-COO)-Ag_3 and COO-Cdot(-COO)-Ag_3 are -3.85 and -4.22 eV respectively. These values are higher than the adsorption energy of α-D-glucose (-0.52 eV) on Ag_3 by a 635 and 705 %, which can cause the replacement of α-D-glucose-Ag_3 [23]. As mentioned, the α-D-glucose molecule acts as capping agent in the synthesis of AgNPs [14], as also does D-gluconate. However this last molecule has adsorption energies of -4.02 and -5.19 eV for D-gluconate(-OH)-Ag_3 and D-gluconate(-COO)-Ag_3 respectively, and the replacement by Cdots would not be stable, at least for D-gluconate(-COO)-Ag_3.

Figure 5 shows the PDOS of the O atom belonging to the –COO and OH-groups and the corresponding Ag atoms participating in the interaction between the Cdots or capping agent molecules with the silver cluster. It can be noted that there is as higher hybridization between Ag and O atoms states for Cdots and D-gluconate around the Fermi level than for α-D-glucose in the interaction with Ag_3 cluster, which leads to a stronger chemical interaction between them. Also, the hybridized states in Cdots and D-gluconate are widely dispersed; on the contrary, α-D-glucose forms localized states by the overlapping of O and Ag states.

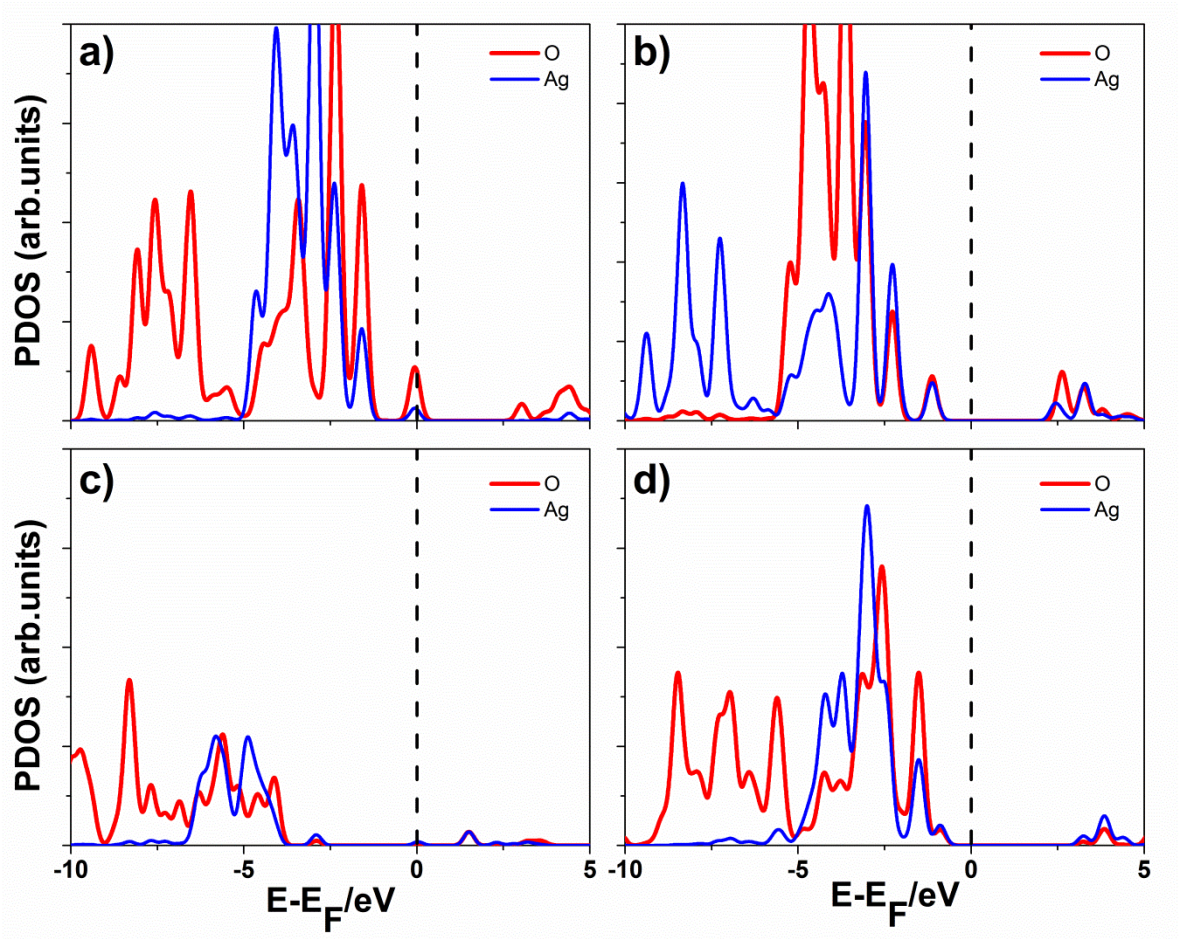

Figure 5 PDOS for Ag and O closest atoms between α-D-glucose, D-gluconate or Cdots and Ag_3 cluster for; a) COO-Cdot(-COO)-Ag_3, b) OH-Cdot(-COO)-Ag_3, c) α-D-glucose-Ag_3 and d) D-gluconate-Ag_3.

A frontier orbital analysis was performed, calculating the HOMO and LUMO isosurfaces for the Cdots and molecules isolated and interacting with silver, which is summarized in **Figure 6**.

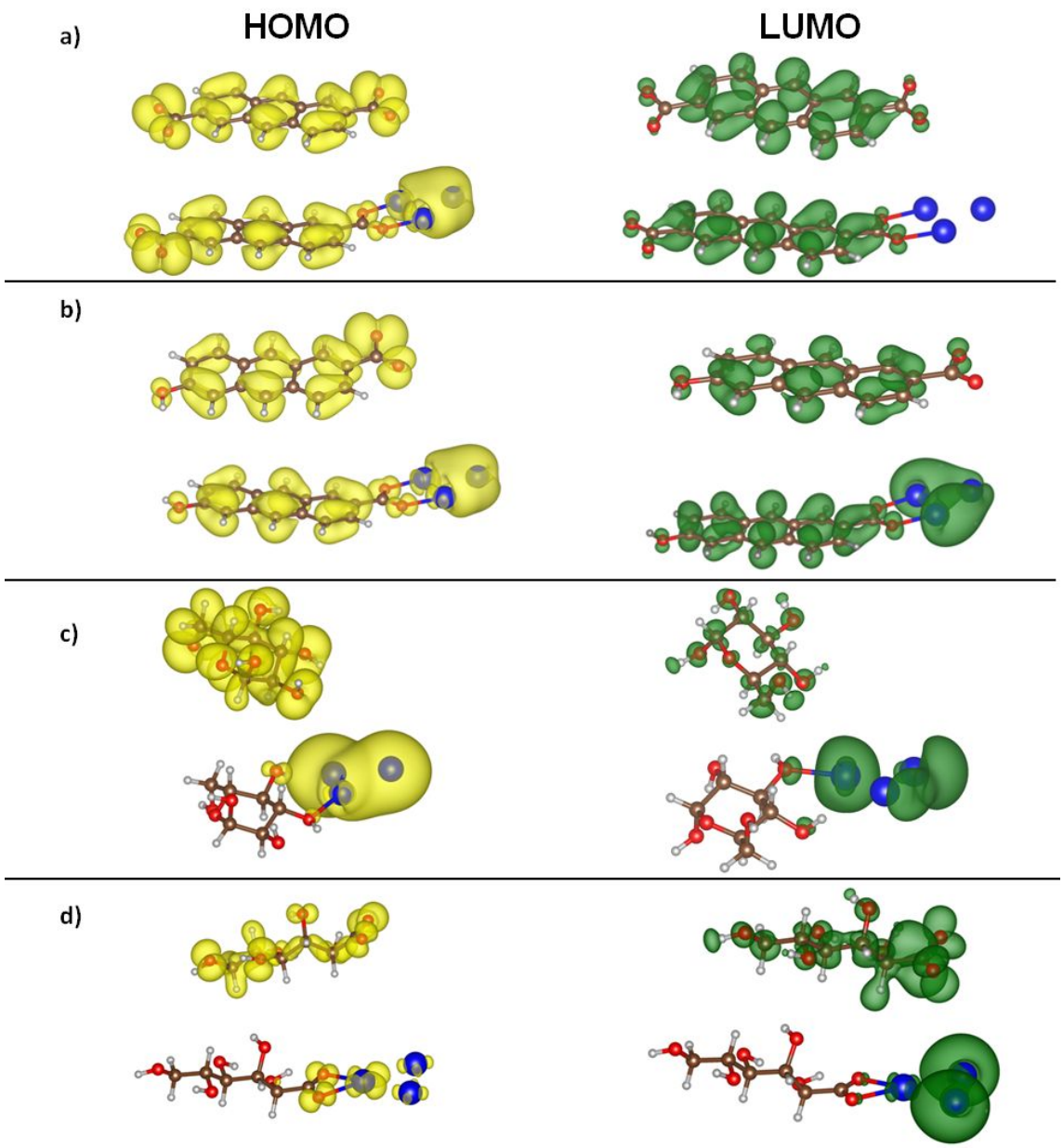

Figure 6 Isosurfaces for HOMO and LUMO states for Cdot structures and molecules involved in the synthesis, before and after the adsorption on Ag_3 cluster; a) COO-Cdot(-COO)-Ag_3, b) OH-Cdot(-COO)-Ag_3, c) α-D-glucose-Ag_3 and d) D-gluconate(-COO)-Ag_3.

As can be observed in **Figure 6** a) and b), the HOMO states concentrate on C and O atoms, and also Ag atoms after the adsorption. The states on C atoms correspond with mainly π molecular orbitals of the carbon rings. Instead, LUMO states correspond mainly with C π* molecular orbitals. After the adsorption, the LUMO states decrease in the Cdots. This is compatible with a charge transfer

from Ag_3 cluster to the Cdot. Concerning the interaction of D-gluconate and the Ag_3 cluster the HOMO states concentrate in the region of interaction between this molecule and Ag_3 cluster. On the other hand LUMO states are centered almost entirely in the cluster and not in the the molecule, meaning that higher charge transfer occurs after the interaction between D-gluconate and silver. Finally, the α-D-glucose HOMO and LUMO states dispersed around the entire molecule, become highly localized on O and Ag atoms after the adsorption as consequence of the localized hybridization nature between α-D-glucose and silver.

In order to obtain a better understanding of the interactions between Cdots and capping agent molecules with AgNPs, BO and OP calculations were carried out for the different systems. The more relevant results for the atoms taken as reference are listed in **Table 1.** C-O indicates the bond belonging to the interacting –COO group in COO-Cdot(-COO)-Ag_3, COO-Cdot(-COO)-Ag_3 and D-gluconate-Ag_3 structures and the bond between C and the –OH group in α-D-glucose-Ag_3. C-C refers to the bond between C and the –COO group for –D-gluconate and Cdots and the O-H refers to bond in the –OH group of α-D-glucose that interacts with Ag_3. Finally Ag-O indicates the bond between –COO or –OH groups and Ag_3. The bonds affected indirectly by the Ag-O interaction are compared with the isolated situation.

Table 1 OP, BO and bond distances for selected pairs of atoms for COO-Cdot(-COO)-Ag_3, OH-Cdot(-COO)-Ag_3, α-D-glucose-Ag_3 and D-gluconate-Ag_3 optimized structures.

System	Atoms	Distance/Å	OP	BO
COO-Cdot(-COO)-Ag_3	**O-Ag**	2.21	0.35	0.49
	C-O	1.28	0.95	1.52
	C-$O_{isolated}$	1.37 (1.22)	0.86(1.11)	1.35 (1.81)
	C-C	1.50	0.62	0.94
	C-$C_{isolated}$	1.48	0.63	0.95
OH-Cdot(-COO)-Ag_3	**O-Ag**	2.21	0.36	0.51
	C-O	1.28	0.95	1.52
	C-$O_{isolated}$	1.37 (1.22)	0.87(1.12)	1.36 (1.80)
	C-C	1.50	0.63	0.94
	C-$C_{isolated}$	1.48	0.64	0.96
α-D-glucose-Ag_3	**O-Ag**	2.31	0.29	0.41
	O-H	0.98	0.48	0.73
	O-$H_{isolated}$	0.98	0.51	0.79
	C-O	1.45	0.67	0.98
	C-$O_{isolated}$	1.43	0.72	1.09
D-gluconate(-COO)-Ag_3	**O-Ag**	2.30	0.30	0.41
	C-O	1.27	0.96	1.54
	C-$O_{isolated}$	1.36 (1.22)	0.85 (1.09)	1.34 (1.78)
	C-C	1.53	0.57	0.84
	C-$C_{isolated}$	1.52	0.58	0.85

The OP, BO and bond distances are approximately equal in the interaction between Ag_3 and –COO group for COO-Cdot(-COO)-Ag_3 and OH-Cdot(-COO)-Ag_3. Both cases present a reduction in the C-C and C-O bond strength with respect to the isolated Cdot, as consequence of the interaction of –COO group with silver. For the C-O bond the value in parenthesis corresponds to a double bond, and it is observed that the interaction with Ag produces a single C-O bond with OP, BO and bond length with values around those obtained for –COO group single and double bonds.

The O-Ag interaction in α-D-glucose and D-gluconate respectively, have approximately the same OP and BO. The difference on the adsorption energies between these two molecules is due to the formation an extra Ag-O bond in D-

gluconate. Again the C-C bond becomes weaker, reducing approximately 0.7 % and 1 % their OP and BO respectively, as consequence of the Ag-O interaction. The C-O bond OP and BO are reduced approximately 12 % and 14 %. In α-D-glucose molecule, O-H and C-O bonds experiment also a decrease in their strength due to the interaction with silver.

Compared to α-D-glucose and D-gluconate, when a Cdot interacts with the Ag3 cluster, the Ag-O bond OP and BO are 18 and 19 % larger. This, in part explains the Cdots major stability compared to α-D-glucose, however it seems to contradict the fact that D-gluconate is energetically more stable than Cdots. This behavior can be explained focusing in the interactions surrounding the Ag-O bond (C-C and C-O bonds) since for Cdots the C-O bond is weaker and especially the C-C OP and BO decrease approximately twice as much as the case for D-gluconate. It is clear from this analysis, that the capping molecules and Cdots have chemical contributions in the interaction with Ag_3 cluster according to the OP and BO calculated parameters.

Density difference analysis was also performed with the aim to examine the charge distribution in the adsorption region. The charge density difference ($\Delta\rho$) isosurface, is obtained as: $\Delta\rho = \rho_{System} - \rho_{Ag_3} - \rho_{Cdot(molecule)}$. In this equation, ρ_{System} represents the charge density of the system formed by Cdot (molecule) adsorbed on the Ag_3 cluster, while ρ_{Ag_3} and $\rho_{Cdot(molecule)}$ indicate the charge density of the isolated Ag_3 cluster and the Cdot (molecule) respectively. The results are shown in Figure 7.

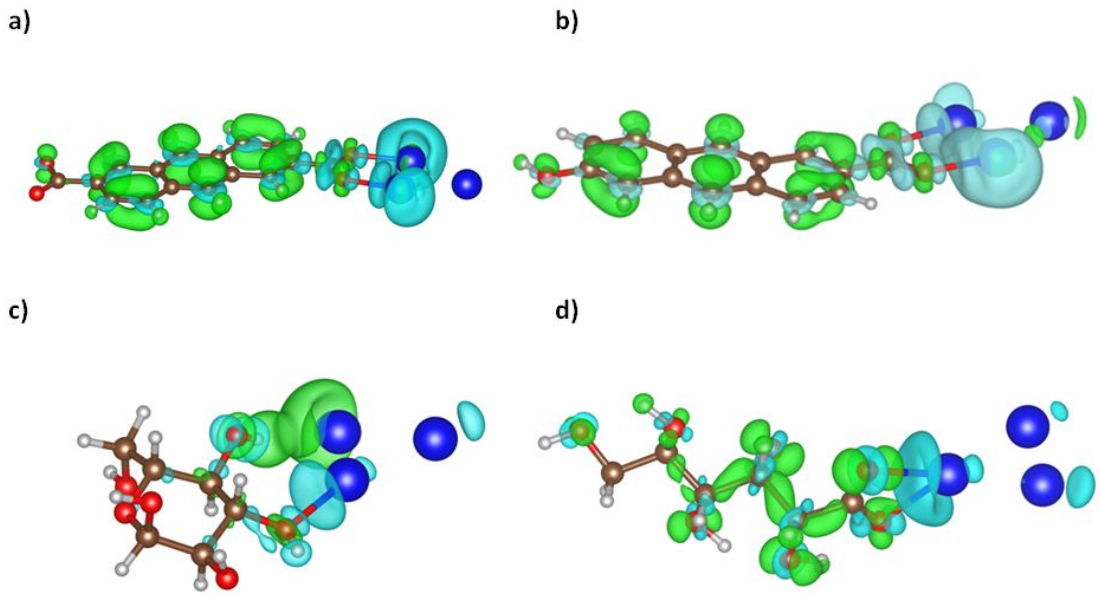

Figure 7 Density difference isosurfaces for a) COO-Cdot(-COO)-Ag_3, b) OH-Cdot(-COO)-Ag_3, c) α-D-glucose-Ag_3 and d) D-gluconate(-COO)-Ag_3 optimized structures. The value for the isosurfaces is equal to 0.02 e $Å^{-3}$. Green and turquoise colors represent accumulation and depletion charge regions respectively.

For Cdots and D-gluconate, after their interaction with silver there is a clear accumulation of charge on them, while a depletion of charge occurs on Ag_3 silver cluster. This is a consequence of a charge transfer from silver to the Cdot or D-gluconate, resulting in an electrostatic interaction between them and Ag_3 cluster which contributes favorably to the stabilization. In the case of α-D-glucose only a charge polarization in the cluster is observed which can interact with the oxygenated group of the molecules that are slightly polarized.

Based on the strong interaction that silver can have with Cdots through –COO groups, calculations of the of the normal modes vibrational frequencies and absorption intensities at these frequencies were performed in order to detect potential changes in Cdots during the interaction with silver. The same analysis was extended to the capping molecules that interact with silver. A comparison of these theoretical results with those obtained from experimental FTIR spectra can be considerably useful to determine if Cdot and silver interaction really takes

place in the Ag@Cdot hybrids structures. **Table 2** reports the normal mode frequencies corresponding to the different system functional groups and their IR absorption relative intensity, which is a measure of the amount of absorption, compared to the isolated Cdot for the same number of molecules per unit volume. In this sense, this last property quantifies the intrinsic tendency of the molecule or Cdots to absorb IR radiation at the obtained frequency for the considered groups.

Table 2 Frequencies and IR relative intensities of absorption obtained by DFT calculations for the vibrational normal modes of –COO and –OH functional groups.

System	Functional group	Stretching Mode	Frequency/cm^{-1}	I_i^{rel}
Cdot	-COO	C-O (mode1)	1699	1.00
		C-O (mode2)	1055	1.00
	-OH	C-O	1019	1.00
Cdot(-COO)-Ag$_3$	-COO	C-O (mode1)	1471	0.87
		C-O (mode2)	1331	1.81
Cdot(-COO)-Ag$_3$	-COO (unbound)	C-O (mode1)	1670	1.01
		C-O (mode2)	1038	0.73
	-OH (unbound)	C-O	1267	1.89
D-gluconate(-OH)-Ag$_3$	-COO (unbound)	C-O (mode1)	1704	0.87
		C-O (mode2)	1151	0.29
D-gluconate(-COO)-Ag$_3$	-COO	C-O (mode1)	1515	0.00
		C-O (mode2)	1387	0.01
	-OH (unbound)	C-O	1325	0.74
α-D-glucose	-OH	C-O	895	0.56
α-D-glucose-Ag$_3$	-OH (unbound)	C-O	1265	0.48

The –COO and -OH groups for the Cdot, have stretching vibration frequencies that are in accordance with experimental and theoretical values reported in literature for these groups [21,49]. Modes one and two for –COO group correspond to symmetrical and asymmetrical stretching vibration. The C-O

stretching normal mode for the group –OH can be related with the peak at 1010 nm signaled in the FTIR spectra (see **Figure 2**). Also, this peak can be attributed to the second mode of the –COO group. On the other hand, the frequency of normal mode 1 of –COO group, can be associated with the peak at 1730 cm^{-1} in FTIR spectra, within a relative error of 1.8 %. The normal modes of these groups are altered when the Cdot (or molecule) is interacting with silver, and also depend on being attached to a molecule or a Cdot. The –COO group directly interacting with silver generates a decrease in the higher frequency and increase in the lower one for both D-gluconate and Cdot. But for the last, and absorption occurs, especially for the normal mode 2, while D-gluconate is not IR active. However, when D-gluconate is adsorbed with a –OH group, which is a possible configuration according to González Fá *et. al.* [14] work, -COO group becomes IR active, mainly mode 1, with an absorption in a frequency close to the higher frequency peak signaled in the FTIR spectra. The stretching frequency of the C-O bond corresponding to the -OH group is also shifted for D-gluconate and Cdot interacting with silver through –COO group, having both species IR absorption.

It is also interesting to analyze the changes in frequencies and absorption intensities of the functional groups when they do not interact directly with silver, since that is a possible configuration in the formation process. **Table 2** shows that the unbound –COO group can have absorption at frequencies 1670 and 1038 cm^{-1}, that match well with the experimental C=O and C-O modes obtained in FTIR spectra. The theoretically intensity is higher for the Cdot than the D-gluconate ion, but this can be also affected by the amount of these compounds around the AgNP. Finally –OH unbound for α-D-glucose adsorbed and not adsorbed, and for D-gluconate and Cdot adsorbed by –COO group, have C-O stretching frequencies between 895 and 1267 cm^{-1}. It is interesting to note that the C-O stretching frequency shifts from approximately 895 to 1265 cm^{-1} for α-D-glucose when this molecule adsorbs. Something similar occurs for the Cdot, with a frequency shift for C-O stretching from approximately 1019 to 1267 cm^{-1} corresponding to not adsorbed and adsorbed Cdot respectively. Additionally both frequencies are IR active, and the intensity is considerably higher for the adsorbed Cdot compared with the adsorbed α-D-glucose. This effect was also indentified in the experimental FTIR *spectra* (see **Figure 2**), where a peak at 1250

cm^{-1} is observed. It has higher absorption for Ag@Cdot compound than for AgNP, which means that effectively an interaction between Cdot and AgNP is occurring in the hybrid structures. Consequently, this level of agreement between the calculation predictions and the spectra measurements constitutes strong evidence that some Cdots are interacting with AgNP surface in the Ag@Cdot structures.

4. CONCLUSION

AgNPs, Cdots and Ag@Cdots with different glucose concentrations were synthesized and characterized by UV Vis, IR, zeta potential and TGA. The experimental results suggest a strong interaction between AgNPs and Cdots in the hybrid nanoparticles. The experimental data could be correlated and interpreted by calculations obtained by DFT. The results suggest an interaction between the $-COO^-$ functional group of the Cdots with AgNPs, which results in the adsorption of the Cdots on the surface of the AgNPs. Strong evidence of the AgNPs and Cdots interaction was found by the detection that –OH group in the Cdots experienced a frequency shift (1267 cm^{-1}) and greater absorption in the IR due to the –COO-Ag interaction, also observed in the experimental IR spectra.

A selective adsorption of the Cdots on AgNPs for hybrid Ag@Cdot structures occurs at lower concentration of glucose, however Cdots can be formed also in the solution when the glucose concentration is increased as the Z potentials analysis suggests. Consequently the AgNPs surface can act as active sites constituting center for formations of Cdots in the hybrid structures. The methodology used in this work is not only useful for this nanoparticle system but could also be used for the study of the interaction between other types of hybrid nanoparticles.

Acknowledgment

We acknowledge the financial support from SGCyT-UNS (PGI–UNS 24/Q097 and PGI-UNS 24/F072) and ANPCyT (PICT-2016-4094). R.E.A., M.E.P and A. J. are members of CONICET and J.M.A. is a Postdoctoral fellow of this institution. M.F. P. is a member of Comisión Investigaciones Científicas pcia. Bs. As. (CIC-BA).

REFERENCES

(1) Wang, J. Nanomaterial-Based Electrochemical Biosensors. **2005**, No. i, 421–426. https://doi.org/10.1039/b414248a.

(2) Tao, Z.; Huang, Y. an; Liu, X.; Chen, J.; Lei, W.; Wang, X.; Pan, L.; Pan, J.; Huang, Q.; Zhang, Z. High-Performance Photo-Modulated Thin-Film Transistor Based on Quantum Dots/Reduced Graphene Oxide Fragment-Decorated ZnO Nanowires. *Nano-Micro Lett.* **2016**, *8* (3), 247–253. https://doi.org/10.1007/s40820-016-0083-7.

(3) Weng, G. E.; Ling, A. K.; Lv, X. Q.; Zhang, J. Y.; Zhang, B. P. III-Nitride-Based Quantum Dots and Their Optoelectronic Applications. *Nano-Micro Lett.* **2011**, *3* (3), 200–207. https://doi.org/10.3786/nml.v3i3.p200-207.

(4) Lim, S. Y.; Shen, W.; Gao, Z. Carbon Quantum Dots and Their Applications. *Chemical Society Reviews*. Royal Society of Chemistry January 7, 2015, pp 362–381. https://doi.org/10.1039/c4cs00269e.

(5) Yang, Z. C.; Wang, M.; Yong, A. M.; Wong, S. Y.; Zhang, X. H.; Tan, H.; Chang, A. Y.; Li, X.; Wang, J. Intrinsically Fluorescent Carbon Dots with Tunable Emission Derived from Hydrothermal Treatment of Glucose in the Presence of Monopotassium Phosphate. *Chem. Commun.* **2011**, *47* (42), 11615–11617. https://doi.org/10.1039/c1cc14860e.

(6) Zong, J.; Zhu, Y.; Yang, X.; Shen, J.; Li, C. Synthesis of Photoluminescent Carbogenic Dots Using Mesoporous Silica Spheres as Nanoreactors. *Chem. Commun.* **2011**, *47* (2), 764–766. https://doi.org/10.1039/c0cc03092a.

(7) Arroyave, M.; Springer, V.; Centurión, M. E. Novel Synthesis Without Separation and Purification Processes of Carbon Dots and Silver/Carbon Hybrid Nanoparticles. *J. Inorg. Organomet. Polym. Mater.* **2019**. https://doi.org/10.1007/s10904-019-01266-1.

(8) Tang, L.; Ji, R.; Cao, X.; Lin, J.; Jiang, H.; Li, X.; Teng, K. S.; Luk, C. M.; Zeng, S.; Hao, J.; et al. Deep Ultraviolet Photoluminescence of Water-Soluble Self-

Passivated Graphene Quantum Dots. *ACS Nano* **2012**, *6* (6), 5102–5110. https://doi.org/10.1021/nn300760g.

(9) Prosposito, P.; Mochi, F.; Ciotta, E.; Casalboni, M.; De Matteis, F.; Venditti, I.; Fontana, L.; Testa, G.; Fratoddi, I. Hydrophilic Silver Nanoparticles with Tunable Optical Properties: Application for the Detection of Heavy Metals in Water. *Beilstein J. Nanotechnol.* **2016**, *7* (1), 1654–1661. https://doi.org/10.3762/bjnano.7.157.

(10) Sanskriti, I.; Upadhyay, K. K. Silver Nanoparticles as Highly Efficient and Selective Optical Probe for Sulphide via Dendrimer Formation in Aqueous Medium. *RSC Adv.* **2016**, *6* (18), 14563–14569. https://doi.org/10.1039/c5ra25625a.

(11) Gurunathan, S.; Park, J. H.; Han, J. W.; Kim, J. H. Comparative Assessment of the Apoptotic Potential of Silver Nanoparticles Synthesized by Bacillus Tequilensis and Calocybe Indica in MDA-MB-231 Human Breast Cancer Cells: Targeting P53 for Anticancer Therapy. *Int. J. Nanomedicine* **2015**, *10*, 4203–4223. https://doi.org/10.2147/IJN.S83953.

(12) Li, W. R.; Xie, X. B.; Shi, Q. S.; Zeng, H. Y.; Ou-Yang, Y. S.; Chen, Y. Ben. Antibacterial Activity and Mechanism of Silver Nanoparticles on Escherichia Coli. *Appl. Microbiol. Biotechnol.* **2010**, *85* (4), 1115–1122. https://doi.org/10.1007/s00253-009-2159-5.

(13) Mukherjee, P.; Ahmad, A.; Mandal, D.; Senapati, S.; Sainkar, S. R.; Khan, M. I.; Parishcha, R.; Ajaykumar, P. V.; Alam, M.; Kumar, R.; et al. Fungus-Mediated Synthesis of Silver Nanoparticles and Their Immobilization in the Mycelial Matrix: A Novel Biological Approach to Nanoparticle Synthesis. *Nano Lett.* **2001**, *1* (10), 515–519. https://doi.org/10.1021/nl0155274.

(14) González Fá, A.; López-Corral, I.; Faccio, R.; Juan, A.; Di Nezio, M. S. Surface Enhancement Raman Spectroscopy and Density Functional Theory Study of Silver Nanoparticles Synthetized with D-Glucose. *J. Raman Spectrosc.* **2018**, *49* (11), 1756–1764. https://doi.org/10.1002/jrs.5466.

(15) Ma, J. L.; Yin, B. C.; Wu, X.; Ye, B. C. Simple and Cost-Effective Glucose Detection Based on Carbon Nanodots Supported on Silver Nanoparticles. *Anal. Chem.* **2017**, *89* (2), 1323–1328. https://doi.org/10.1021/acs.analchem.6b04259.

(16) Gurunathan, S.; Han, J. W.; Kim, E. S.; Park, J. H.; Kim, J. H. Reduction of Graphene Oxide by Resveratrol: A Novel and Simple Biological Method for the Synthesis of an Effective Anticancer Nanotherapeutic Molecule. *Int. J. Nanomedicine* **2015**, *10*, 2951–2969. https://doi.org/10.2147/IJN.S79879.

(17) Sapsford, K. E.; Tyner, K. M.; Dair, B. J.; Deschamps, J. R.; Medintz, I. L.

Analyzing Nanomaterial Bioconjugates: A Review of Current and Emerging Purification and Characterization Techniques. *Anal. Chem.* **2011**, *83* (12), 4453–4488. https://doi.org/10.1021/ac200853a.

(18) Gaigeot, M.-P.; Sprik, M. Ab Initio Molecular Dynamics Computation of the Infrared Spectrum of Aqueous Uracil. *J. Phys. Chem. B* **2003**, *107* (38), 10344–10358. https://doi.org/10.1021/jp034788u.

(19) Gaigeot, M. P. Theoretical Spectroscopy of Floppy Peptides at Room Temperature. A DFTMD Perspective: Gas and Aqueous Phase. *Phys. Chem. Chem. Phys.* **2010**, *12* (14), 3336–3359. https://doi.org/10.1039/b924048a.

(20) Brauer, B.; Pincu, M.; Buch, V.; Bar, I.; Simons, J. P.; Gerber, R. B. Vibrational Spectra of α-Glucose, β-Glucose, and Sucrose: Anharmonic Calculations and Experiment. *J. Phys. Chem. A* **2011**, *115* (23), 5859–5872. https://doi.org/10.1021/jp110043k.

(21) Timofeeva, T. E.; Egorova, M. N.; Tomskaya, A. E.; Smagulova, S. A. Ab Initio Calculations of Energy and IR Spectra of Edge Functionalized Graphene Quantum Dots. In *AIP Conference Proceedings*; American Institute of Physics Inc., 2018; Vol. 2041. https://doi.org/10.1063/1.5079350.

(22) Tran, N. A.; Lee, C.; Lee, D. H.; Cho, K. H.; Joo, S. W. Water Molecules on the Epoxide Groups of Graphene Oxide Surfaces. *Bull. Korean Chem. Soc.* **2018**, *39* (11), 1320–1323. https://doi.org/10.1002/bkcs.11600.

(23) Ambrusi, R. E.; Arroyave, J. M.; Centurión, M. E.; Di Nezio, M. S.; Pistonesi, M. F.; Juan, A.; Pronsato, M. E. Density Functional Theory Model for Carbon Dot Surfaces and Their Interaction with Silver Nanoparticles. *Phys. E Low-dimensional Syst. Nanostructures* **2019**, *114*, 113640. https://doi.org/10.1016/j.physe.2019.113640.

(24) González Fá, A. J.; Juan, A.; Di Nezio, M. S. Synthesis and Characterization of Silver Nanoparticles Prepared with Honey: The Role of Carbohydrates. *Anal. Lett.* **2017**, *50* (5), 877–888. https://doi.org/10.1080/00032719.2016.1199558.

(25) Kresse, G.; Furthmüller, J. Efficient Iterative Schemes for Ab Initio Total-Energy Calculations Using a Plane-Wave Basis Set. *Phys. Rev. B - Condens. Matter Mater. Phys.* **1996**, *54* (16), 11169–11186. https://doi.org/10.1103/PhysRevB.54.11169.

(26) Kresse, G.; Furthmüller, J. Efficiency of Ab-Initio Total Energy Calculations for Metals and Semiconductors Using a Plane-Wave Basis Set. *Comput. Mater. Sci.* **1996**, *6* (1), 15–50. https://doi.org/10.1016/0927-0256(96)00008-0.

(27) Perdew, J. P.; Burke, K.; Ernzerhof, M. Generalized Gradient Approximation Made Simple. *Phys. Rev. Lett.* **1996**, *77* (18), 3865–3868.

https://doi.org/10.1103/PhysRevLett.77.3865.

(28) Blöchl, P. E. Projector Augmented-Wave Method. *Phys. Rev. B* **1994**, *50* (24), 17953–17979. https://doi.org/10.1103/PhysRevB.50.17953.

(29) Joubert, D. From Ultrasoft Pseudopotentials to the Projector Augmented-Wave Method. *Phys. Rev. B - Condens. Matter Mater. Phys.* **1999**, *59* (3), 1758–1775. https://doi.org/10.1103/PhysRevB.59.1758.

(30) Monkhorst, H. J.; Pack, J. D. Special Points for Brillouin-Zone Integrations. *Phys. Rev. B* **1976**, *13* (12), 5188–5192. https://doi.org/10.1103/PhysRevB.13.5188.

(31) Press, W. H.; Teukolsky, S. A.; Vetterling, W. T.; Flannery, B. P. Numerical Recipes in C (Second Edition). In *Numerical Recipes in C (Second edition)*; Cambridge University Press: Cambridge, 1992; pp 408–412.

(32) Grimme, S. Semiempirical GGA-Type Density Functional Constructed with a Long-Range Dispersion Correction. *J. Comput. Chem.* **2006**, *27* (15), 1787–1799. https://doi.org/10.1002/jcc.20495.

(33) Paier, J.; Marsman, M.; Kresse, G. Why Does the B3LYP Hybrid Functional Fail for Metals? *J. Chem. Phys.* **2007**, *127* (2). https://doi.org/10.1063/1.2747249.

(34) Mathew, K.; Sundararaman, R.; Letchworth-Weaver, K.; Arias, T. A.; Hennig, R. G. Implicit Solvation Model for Density-Functional Study of Nanocrystal Surfaces and Reaction Pathways. *J. Chem. Phys.* **2014**, *140* (8), 084106. https://doi.org/10.1063/1.4865107.

(35) Mathew, K.; Hennig, R. G. Implicit Self-Consistent Description of Electrolyte in Plane-Wave Density-Functional Theory. **2016**.

(36) Rekha, T. N.; Rajkumar, B. J. M. Density Functional Theory Study on Silver Clusters Using Dimers, Trimers, and Tetramers as Building Units. *Can. J. Phys.* **2015**, *93* (3), 318–325. https://doi.org/10.1139/cjp-2014-0256.

(37) Hoffmann, R. *Solids and Surfaces : A Chemist's View of Bonding in Extended Structures*.

(38) Dronskowski, R.; Hoffmann, R. *Computational Chemistry of Solid State Materials: A Guide for Materials Scientists, Chemists, Physicists and Others: A Guide for Material Scientists, Chemists, Physicists and Others*; Wiley-VCH, 2005.

(39) Limas, N. G.; Manz, T. A. Introducing DDEC6 Atomic Population Analysis: Part 2. Computed Results for a Wide Range of Periodic and Nonperiodic Materials. *RSC Adv.* **2016**, *6* (51), 45727–45747. https://doi.org/10.1039/c6ra05507a.

(40) Manz, T. A.; Limas, N. G. Introducing DDEC6 Atomic Population Analysis: Part 1. Charge Partitioning Theory and Methodology. *RSC Adv.* **2016**, *6* (53), 47771–47801. https://doi.org/10.1039/c6ra04656h.

(41) Manz, T. A.; Limas, N. G. Chargemol program for performing DDEC analysis, Version 3.4.4, 2016 - Browse Files at SourceForge.net

(42) Sholl, D. S.; Steckel JA. *Density Functional Theory; a Practical Introduction, John Wiley & Sons, Inc., Canada*; 2009; Vol. John Wile.

(43) Jackson, K.; Pederson, M. R. Density-Functional-Based Predictions of Raman and IR Spectra for Small Si Clusters. *Phys. Rev. B - Condens. Matter Mater. Phys.* **1997**, *55* (4), 2549–2555. https://doi.org/10.1103/PhysRevB.55.2549.

(44) Porezag, D.; Pederson, M. R. Infrared Intensities and Raman-Scattering Activities within Density-Functional Theory. *Phys. Rev. B - Condens. Matter Mater. Phys.* **1996**, *54* (11), 7830–7836. https://doi.org/10.1103/PhysRevB.54.7830.

(45) Wilson, E. *Molecular Vibrations : The Theory of Infrared and Raman Vibrational Spectra*; McGraw-Hill: New York, 1955.

(46) Garcia, M. A. Surface Plasmons in Metallic Nanoparticles: Fundamentals and Applications. *Journal of Physics D: Applied Physics*. July 20, 2011. https://doi.org/10.1088/0022-3727/44/28/283001.

(47) Song, H.; Huang, J.; Jia, X.; Sheng, W. Facile Synthesis of Core-Shell Ag@C Nanospheres with Improved Tribological Properties for Water-Based Additives. *New J. Chem.* **2018**, *42* (11), 8773–8782. https://doi.org/10.1039/c8nj01382a.

(48) Ahmadian-Fard-Fini, S.; Salavati-Niasari, M.; Ghanbari, D. Hydrothermal Green Synthesis of Magnetic Fe3O4-Carbon Dots by Lemon and Grape Fruit Extracts and as a Photoluminescence Sensor for Detecting of E. Coli Bacteria. *Spectrochim. Acta - Part A Mol. Biomol. Spectrosc.* **2018**, *203* (2017), 481–493. https://doi.org/10.1016/j.saa.2018.06.021.

(49) Stuart, B. H. *Infrared Spectroscopy: Fundamentals and Applications*; wiley, 2005. https://doi.org/10.1002/0470011149.

(50) Pal, T.; Mohiyuddin, S.; Packirisamy, G. Facile and Green Synthesis of Multicolor Fluorescence Carbon Dots from Curcumin: In Vitro and in Vivo Bioimaging and Other Applications. *ACS Omega* **2018**, *3* (1), 831–843. https://doi.org/10.1021/acsomega.7b01323.

(51) Antelo, J.; Avena, M.; Fiol, S.; López, R.; Arce, F. Effects of PH and Ionic Strength on the Adsorption of Phosphate and Arsenate at the Goethite-Water Interface. *J. Colloid Interface Sci.* **2005**, *285* (2), 476–486. https://doi.org/10.1016/j.jcis.2004.12.032.

(52) Waiman, C. V; Avena, M. J.; Regazzoni, A. E.; Zanini, G. P. A Real Time in Situ ATR-FTIR Spectroscopic Study of Glyphosate Desorption from Goethite as Induced by Phosphate Adsorption: Effect of Surface Coverage. *J. Colloid*

32

Interface Sci. **2013**, *394*, 485–489. https://doi.org/10.1016/j.jcis.2012.12.063.